Giant reduction and tunability of the thermal conductivity of carbon nanotubes through low-frequency resonant modes

Ashutosh Giri and Patrick E. Hopkins

Phys. Rev. B **98**, 045421 — Published 20 July 2018

DOI: 10.1103/PhysRevB.98.045421

Giant reduction and tunability of the thermal conductivity of carbon nanotubes through low frequency resonant modes

Ashutosh Giri[1,*] and Patrick E. Hopkins[1,2,3,†]

[1]*Department of Mechanical and Aerospace Engineering, University of Virginia, Charlottesville, Virginia 22904, USA*
[2]*Department of Materials Science and Engineering, University of Virginia, Charlottesville, Virginia 22904, USA*
[3]*Department of Physics, University of Virginia, Charlottesville, Virginia 22904, USA*

Manipulating thermal transport by designing materials with control of their vibrational properties over the entire spectral range of frequencies would provide a unique path to create solids with designer thermal conductivity. Traditional routes of nanostructuring to reduce the vibrational thermal conductivity of solids only target narrow bands of vibrational energy spectrum, which is often based on the characteristics dimensions of the nanostructure. In this work, we demonstrate the ability to simultaneously impact the phonon transport of both high and low frequency modes by creating defects that act as both high frequency phonon scattering sites while coherently manipulating low frequency waves via resonance with the long wavelength phonons. We use atomistic simulations to identify fullerenes functionalized on the side walls of carbon nanotubes (CNT) as efficient phonon blocks realized through localized resonances that appear due to hybridization between the modes of the fullerene and the underlying CNT. We show that with a large surface coverage and high periodicity in the inclusion of the covalently bonded fullerenes, the thermal conductivity of individual CNTs can be lowered by more than an order of magnitude, thus providing a large tunability in the thermal transport across these novel materials. We prescribe the large reduction in thermal conductivity to a combination of resonant phonon localization effects leading to phonon band anticrossings and vibrational scattering effects due to the inclusion of the strongly bonded fullerene molecules.

I. INTRODUCTION

The most often used course to reduce thermal transport in semiconducting solids is by nanostructuring and exploiting phonon scattering at interfaces and/or defect sites.[1,2] Generally nanostructuring approaches lead to scattering of high frequency phonons while low frequency phonons with long mean-free-paths (that have been shown to contribute significantly to heat conduction[3–5]) are mostly left unimpeded.[6,7] While hierarchical approaches have been used to efficiently scatter a larger spectral bandwidth of vibrational energy carriers,[6–8] still the characteristic lengths of the hierarchical nanostructures do not effectively suppress the long wavelength phonon transport to realize the full potential for large reductions in thermal conductivity.[6,7,9–11] In this context, phononic metamaterials based on silicon have been proposed to effectively scatter low-frequency phonons by resonant effects.[12–14] The metamaterials scatter phonons via structural rather than compositional effects since these resonators are placed as pillars on the outer walls of the solid membranes. These attached nanoresonators introduce standing waves that hybridize with the modes in the underlying membrane, which gives rise to avoided level crossings and localized modes characterized by flat bands in the phonon dispersion relation with greatly reduced group velocities and consequently reduced thermal conductivities.[12] This localized resonant method allows for the manipulation of waves with characteristic wavelengths that are several times larger than the characteristic dimensions of the resonators,[15] thus offering a unique way to manipulate acoustic as well as thermal transport properties in materials. In this work, we use the concept of localized resonances and hybridization to show that the thermal conductivities in an organic-based new class of materials termed 'nanobuds', where fullerene molecules are wielded on to single-walled carbon nanotubes (CNTs), are greatly reduced.

Individual CNTs possess exceptionally high thermal conductivity of $\sim$3000 W m^{-1} K^{-1} or higher at room temperature,[16–18] which makes them attractive candidates for understanding their fundamental materials thermophysics as well as for usage in practical applications such as energy storage and thermal management.[19–22] However, owing to their chemical neutrality, CNTs are difficult to combine with other materials and fractures upon compaction.[23] To circumvent these issues, chemically active C_{60} molecules have been covalently attached on the side walls of single-walled CNTs (also known as 'nanobuds') to increase their chemical reactivity and mechanical flexibility.[24,25] The nanobud structures exhibit extremely high current density, are optically transparent and are readily accessible by experimental synthesis.[26] Along with the enhancement in their physical properties, fullerene functionalization also prevents slippage in hybrid CNT materials making them immobile as opposed to the mobile character of fullerene and CNTs.[27] However, the complete understanding of thermal transport in these hybrid materials comprising of chemically functionalized CNTs with fullerene molecules has been largely unexplored, thus leaving a void in our understanding of the basic science in their vibrational energy transport and preventing their material design for practical interests (for example, in flexible microelectronic devices[28]).

In this work, we perform a systematic study of the influence of covalently bonded C_{60} molecules on the surface of CNTs on their thermal transport properties through a series of molecular dynamics (MD) and lattice dynamics (LD) calculations. Equilibrium molecular dynamics (EMD) simulations are utilized to predict the thermal conductivities of functionalized CNTs with the introduction of fullerenes at different periodicities and surface coverages for a range of temperature. We

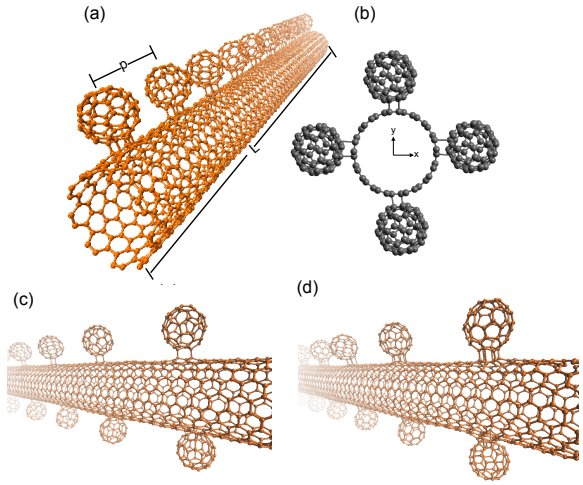

Figure 1. (a) Schematic of a computational domain for a 1-sided nanobud with periodic inclusion of fullerene molecules covalently bonded on the side wall of a carbon nanotube. (b) Schematic of the front view of a 4-sided nanobud. Nanobud structures formed by (c) [2+2] and (d) [6+6] cycloadditions are also shown.

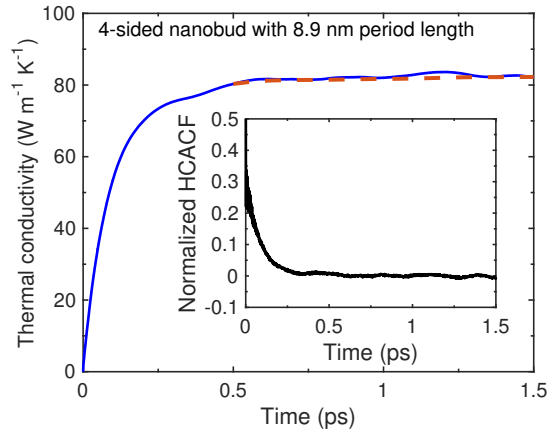

Figure 2. Converged value of thermal conductivity for a 4-sided nanobud with 8.9 nm period length calculated from the integral of the heat current autocorrelation function for a total of 1.5 ps as shown in the inset.

find that the thermal conductivity of individual CNTs can be reduced by more than an order of magnitude at room temperature, thus realizing a large tunability in thermal transport of individual CNTs with periodic inclusion of covalently bonded fullerene molecules on their side walls. We prescribe the large reduction in thermal conductivity to a combination of resonant phonon localization effects leading to phonon band anticrossings and vibrational scattering effects due to the inclusion of the strongly bonded fullerene molecules.

II. METHODOLOGY

The axis of the single-walled CNTs are oriented in the z-direction and periodic boundary conditions are only applied in this direction, thus simulating CNTs with no ends. Consistent with other studies on the thermal transport across CNTs, the Tersoff potential is utilized to describe the interatomic interactions.[29,30] The non-bonded interactions are defined via the Lennard-Jones potential. Fullerene molecules are covalently bonded through periodic inclusions to form carbon nanobuds and periods ranging from ∼1.2 nm to 18 nm are considered. Along with varying periods, we also consider a single, double and four-sided fullerene functionalization to assess the role of surface coverage on thermal transport. A schematic of a 1-sided nanobud is shown in Fig. 1(a) and the front view of a 4-sided nanobud is shown in Fig. 1(b). The length of the simulation cell, L, in the z-direction depends on the periodicity of the fullerene inclusion and are also carefully chosen so as to produce converged values of thermal conductivities for all structures. To predict the thermal conductivities, we utilize the Green-Kubo (GK) approach under the EMD simulations framework. All MD simulations are performed with the LAMMPS code[31] and the lattice dynamics calculations are carried out with GULP.[32]

Our carbon nanotubes (CNTs) have a (9,9) chirality and the addition of the fullerene on the side walls of the CNTs is carried out via the [6+6] cycloaddition.[33] This procedure entails bond formations of the hexagonal face of C_{60} and a hexagonal ring in the single-walled CNT connected together to form six C–C covalent bonds. Density functional calculations have shown this procedure to form stable nanobud structures.[33] Similar stable structures were also formed by [2+2] cycloaddition, where only 2 covalent bonds are formed between the fullerene and the CNT. Examples of the cycloadditions are shown in Figs. 1c and 1d for the [6+6] and [2+2] cycloadditions, respectively. We have calculated the thermal conductivity of both types of stable structures as we will discuss below.

The thermal conductivities of our single-walled carbon nanotube and the nanobud structures are calculated in the axial (α) direction as,

$$\kappa_\alpha = \frac{1}{k_{\mathrm{B}} V T^2} \int_0^\infty \langle S_\alpha(t) S_\alpha(0) \rangle dt, \qquad (1)$$

where t is the time, T and V are the temperature and volume of the system under consideration, respectively, and $\langle S_\alpha(t) S_\alpha(0) \rangle$ is the αth component of the heat current autocorrelation function (HCACF).[34–37] The heat current is calculated every 10 time steps during the data collection period for a total of 1.5 ps. The integration is carried out until the HCACF completely decays to zero. An example of the calculated HCACF as a function of time for a 4-sided nanobud structure with 8.9 nm period length is shown in the inset of Fig. 2 where the HCACF decays to zero by 0.5 picosecond but we average the thermal conductivity (calculated from the integral of the HCACF) from 0.5 ps to 1.5 ps to get a converged value as shown in Fig. 2. If all the available vibrational modes are not included in the simulation cell, the EMD simulations can result in size effects affecting the calculated

thermal conductivities.[38] Therefore, we check for computational domain size effects by conducting GK simulations on domains with different lengths, L, in the axial direction of the carbon nanotubes. For the shorter period lengths ($p < 4$ nm), we use $L \sim$30 nm, which is long enough to produce converged thermal conductivities for all nanobuds. Similarly, for period lengths $p > 4$ nm, we use $L \sim 100$ nm to achieve converged values of thermal conductivities. For statistical uncertainty, we perform 3 different simulations with varying initial conditions for all period lengths and surface coverages.

To calculate the lower limit to thermal conductivity contribution from each mode, we utilize the Allen-Feldman (AF)-theory, which computes the contribution from diffusive and nonpropagating modes as,[39,40]

$$\kappa_{\mathrm{AF}} = \sum_{\mathrm{diffusons}} = \frac{k_{\mathrm{B}}}{V} D_{\mathrm{AF},n}(\omega_n), \qquad (2)$$

where ω_n is the frequency of the nth diffuson and $D_{\mathrm{AF},n}$ under the harmonic approximation is calculated as,

$$D_{\mathrm{AF},n}(\omega_n) = \frac{\pi V^2}{\hbar^2 \omega_n^2} \sum_{m \neq n} |S_{nm}|^2 \delta(\omega_n - \omega_m), \qquad (3)$$

where $|S_{nm}|$ is the heat current operator for the harmonic modes. The Lorentzian broadening of the delta function must be several times greater than the average mode spacing, δ_{avg}. For our calculations, we set the broadening to $5\delta_{\mathrm{avg}}$ to satisfy this criteria; note, perturbing the broadening has negligible affect on the thermal conductivity predicted by the Allen-Feldman theory described in Eq. 2.

Figure 3 shows the thermal conductivity of (9,9) single-walled CNT predicted from our EMD approach as a function of domain length, L. For the thermal conductivity calculations, we specify the cross-sectional area of the CNT as, A=$\sqrt{3}(d_{\mathrm{CNT}} + b)^2/2$, where d_{CNT} is the diameter of the (9,9) CNT and $b = 3.4$ Å is the van der Waals thickness.[45] We note that this definition of the CNT cross-sectional area might be different for similar CNTs in prior literature, which can lead to vastly different thermal conductivity predictions. Along with the cross-sectional area, the choice of the potential and the simulation method used can also impact the MD-predicted thermal conductivities. For example, Salaway *et al.*[44] have comprehensively shown that for a given length of single-walled CNT, the thermal conductivity can range from $\sim$ 225 to 895 W m^{-1} K^{-1} with the choice of the interatomic potential utilized. The choice of the method used to calculate the thermal conductivity of the CNT can also result in varying thermal conductivity predictions. For example, the nonequilibrium MD (NEMD) approach with heat baths and fixed boundary conditions at either end of the computational domain can result in additional phonon scattering at these boundaries, which leads to reduced thermal conductivities as compared to that of the bulk. However, Lukes *et al.*[41] predicted a thermal conductivity of 160 W m^{-1} K^{-1} for a single-walled CNT at room temperature using the EMD approach with periodic boundary conditions (mimicking an infinitely long CNT described by the Reactive Empirical Bond Order (REBO) potential[46]), whereas, Moreland *et al.*[42] and Maruyama *et al.*[43] used NEMD simulations to find higher values of 215 W m^{-1} K^{-1} and 321 W m^{-1} K^{-1} utilizing the Tersoff-Brenner potential, respectively.[47] Considering these differences in the predicted thermal conductivities, another important factor is the domain length where the thermal conductivity increase with the length of the single-walled CNT was shown for both periodic (EMD) and free boundary conditions (NEMD) by Lukes *et al.*[41] In this regard, even a converged and "correct" value of thermal conductivity predicted via the EMD approach with periodic boundary conditions can result in an underestimation of the thermal conductivity. This could explain the order of magnitude difference between the experimentally determined values and those that are predicted via MD since in experiments the lengths of the CNTs can be several microns, whereas in simulations the lengths are mostly limited to the tens or hundreds of nanometers range. Considering the computational efficiency and cost, we note that we do not attempt to calculate the thermal conductivity of CNTs that are several microns long to replicate the experimental results. However, we note that our predicted thermal conductivity for the (9,9) single-walled CNT of $\sim$275 W m^{-1} K^{-1} is similar to the MD-predicted values in the prior literatures as mentioned above. Moreover, since the main goal of this work is to compare and investigate the systematic effect of fullerene addition on the CNT walls, we refrain from trying to consolidate and explain the differences between all the prior literature on the thermal conductivity of single-walled CNT and refer the readers to Refs. 41 and 44 for a detailed investigation into this topic. To gain further confidence in our approach to calculating thermal conductivities of CNTs, we also plot the domain

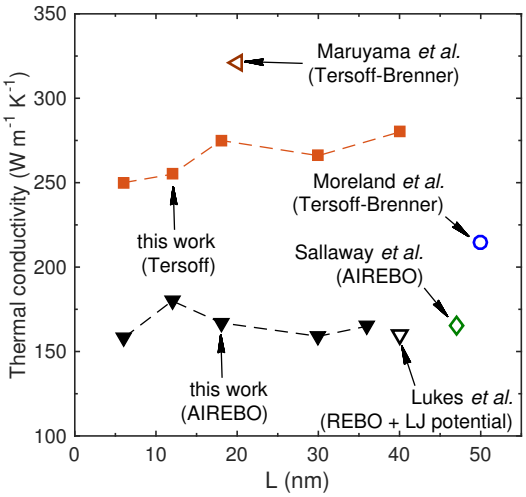

Figure 3. Thermal conductivity of (9,9) single-walled CNT as a function of length, L, predicted via the Green-Kubo approach (solid symbols) with the Tersoff and AIREBO potentials. For comparison, the thermal conductivity of (10,10) single-walled CNT predicted via MD taken from Lukes *et al.*[41], Moreland *et al.*[42], Maruyama *et al.*[43], and Salaway *et al.*[44] along with their respective potentials used are also shown.

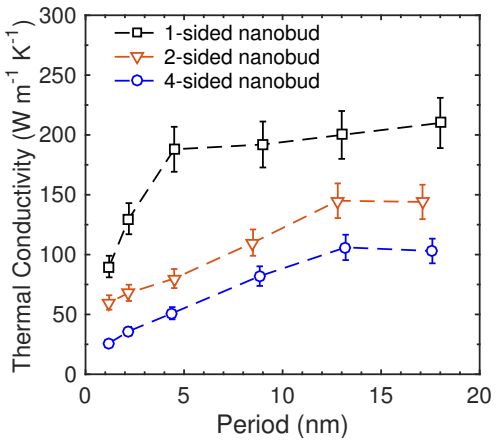

Figure 4. Thermal conductivity of the 1-, 2-, and 4-sided nanobud as a function of period length.

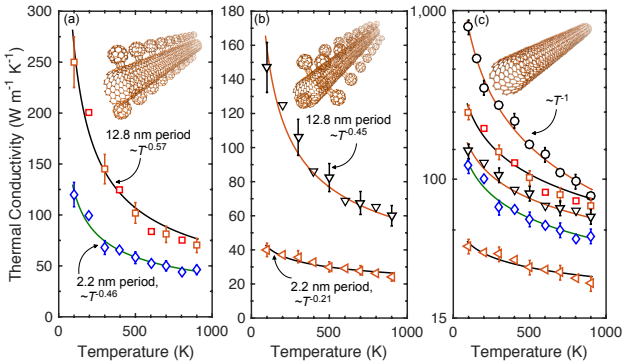

Figure 5. Temperature dependent thermal conductivities for (a) 2-sided (b) 4-sided nanobuds with various period lengths. (c) Thermal conductivity vs. temperature for a pristine carbon nanotube without fullerene functionalization.

length dependent thermal conductivity of our single-walled CNT as described by the Adaptive Intermolecular Reactive Empirical Bond Order (AIREBO) potential (solid triangles) in Fig. 3 for comparison. As is clear, the values predicted via our GK approach match very well with those reported in prior MD works that utilize similar force-fields.

III. RESULTS AND DISCUSSIONS

Figure 4 shows the thermal conductivity of the 1, 2 and 4-sided nanobuds as a function of period length at 300 K. For reference, our calculated thermal conductivity via the same EMD approach of a pristine CNT is ∼275 W m^{-1} K^{-1} at 300 K. As mentioned above, the MD-predicted thermal conductivities of single-walled CNTs in prior literature span an order of magnitude due to variations in computational setups and parameters adopted in the different studies.[41,44] As our primary objective is to investigate the effect of fullerene functionalization on the thermal transport properties of CNTs, we do not try to resolve the discrepancies in the literature values of thermal conductivity of single-walled CNTs and rather focus on the comparative results for our CNT and nanobuds. The thermal conductivity of our nanobuds with short period lengths are much lower as compared to that of the pristine CNT. The decrease in period length monotonically decreases the thermal conductivity for all nanobud types as shown in Fig. 4; the thermal conductivity starts to level-off as the periodicity is increased. Furthermore, as greater number of fullerene molecules are periodically introduced, the thermal conductivity decreases further – a consequence of increased reduction in group velocities due to enhanced hybridization of energy states as will be discussed in detail later. The thermal conductivity of the 4-sided nanobud with a period length of 1.2 nm is 25.8±2.6 W m^{-1} K^{-1}, which is more than an order of magnitude lower than our calculated thermal conductivity for a pristine CNT at 300 K.

Figure 5(a) and 5(b) show the temperature dependent thermal conductivities for the 2- and 4-sided nanobuds with 13.2 nm and 2.2 nm period lengths, respectively. For comparison, the temperature dependent thermal conductivity for a pristine CNT is also shown in Fig. 5(c); we plot the temperature dependent thermal conductivity for the 2- and 4-sided nanobuds as shown in Figs. 5(a) and 5(b), respectively, on a log scale in Fig. 5(c) to highlight the lack of $\sim T^{-1}$ dependence for these nanobuds. As compared to the reduction in thermal conductivity of ∼66% from 100 K to room temperature for a pristine CNT, the reductions in the nanobuds' thermal conductivities are much less pronounced. Moreover, the longer period nanobuds (13.2 nm) as compared to the shorter period nanobuds (2.2 nm) demonstrate larger reductions in thermal conductivity for the range of temperature investigated. Consistent with the findings at moderate temperatures from prior theoretical work considering three-phonon scattering processes,[48] the temperature dependence of thermal conductivity for pristine CNTs are largely driven by anharmonic Umklapp scattering processes as suggested by the $\sim T^{-1}$ dependence.[49] As mentioned above, the $\sim T^{-1}$ trend can no longer explain the results for our nanobuds as shown by the differing temperature dependence fits in Figs. 5(a) and 5(b). However, since the fullerene molecules efficiently block the low frequency phonons and partially scatter the higher frequency modes (as will be discussed in detail later), anharmonic effects are still prevalent, especially for the 2-sided nanobud with 13.2 nm period length (as shown by the relatively more pronounced temperature dependence in Fig. 5(a) for the nanobud with 13.2 nm period compared to the results for other nanobuds). This is because anharmonicity largely affects higher frequency phonons at higher temperatures and thus a larger surface coverage of fullerenes on CNT scatters higher frequency phonons more efficiently. This is exemplified by the lack of temperature dependence of thermal conductivity for our 2.2 nm period, 4-sided nanobud as shown by the $\sim T^{-0.21}$ trend in Fig. 5(b).

We note that the Tersoff potential does not take into account the dependence on dihedral angles. However, the use of

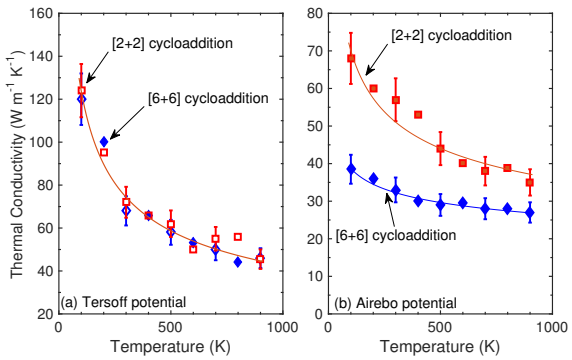

Figure 6. Temperature dependent thermal conductivities for 2-sided nanobuds with 2.2 nm period length prepared via the [2+2] and [6+6] cycloadditions as described by the (a) Tersoff and (b) AIREBO potentials.

a potential such as the AIREBO model,[50] which implements the torsional four-body potential for all dihedrals can lead to significantly reduced thermal conductivities. Figure 6 shows the temperature dependent thermal conductivity for nanobuds prepared from the [2+2] and [6+6] cycloadditions calculated from Tersoff (Fig 6a) and AIREBO (Fig 6b) potentials. Note, the attachment of the fullerenes on the CNT side walls leads to the transformation of the in-plane sp^2 C–C bonds into out-of-plane sp^3-like C–C bonds.[51,52] For both the functionalizations, the nanobuds have fullerenes on 2-sides of the single-walled CNT with 2.2 nm period thicknesses. For the nanobuds described by the Tersoff potential as shown in Fig. 6a, the thermal conductivities over the entire range of temperature are similar for the two cases within uncertainties, suggesting that the method of preparation (whether [2+2] or [6+6] cycloadditions) has negligible influence on the GK-predicted thermal conductivities. However, for nanobuds described by the AIREBO potential,[50] the two methods for nanobud preparation results in different thermal conductivities and their respective temperature trends as shown in Fig. 6b. This can be attributed to the fact that the AIREBO potential takes into consideration an additional torsional term, which is an explicit 4-body potential. The torsional term leads to higher scattering of vibrations at the sp^3-like C–C bonds and the concomitant reduction in the thermal conductivity for the nanobuds prepared by the [6+6] cycloadditions compared to that of the nanobuds formed via [2+2] cycloadditions (with fewer sp^3 bonds in comparison) as shown in Fig. 6b.

To investigate the origin of the large thermal conductivity reduction of our nanobuds in more detail, we calculate the dispersion relations of different structures via harmonic LD calculations. The results are shown in Figs. 7(a) for a 1-sided nanobud with 4.5 nm period length, 7(b) for a 1-sided nanobud with 2.2 nm period length and 7(c) for a 4-sided nanobud with 2.2 nm period length. With the inclusion of the fullerenes on the CNT surface, a series of resonant flat bands crossing the entire Brillouin zone are introduced throughout the spectrum, i.e., at both subwavelength and superwavelength frequencies. The resonant modes hybridize with the underlying acoustic

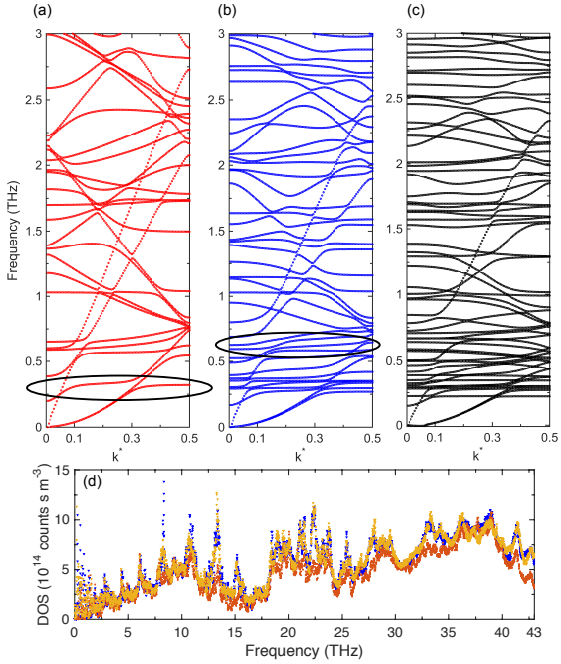

Figure 7. Phonon dispersions calculated via harmonic lattice dynamics calculations in the 0 to 3 THz frequency range for (a) 1-sided nanobud with 4.5 nm period length, (b) 2-sided nanobud with 2.2 nm period length and (c) 4-sided nanobud with 2.2 nm period length. (d) The vibrational density of states for the entire phonon frequency range for the three structures described earlier showing no apparent differences.

and optical modes of the CNT due to band anticrossing effects. This is characterized by the splitting of frequencies into up and down branches leading to mini band gaps with widths dictated by the coupling strength of the resonant and underlying CNT modes. The strong covalent bonds between the CNT and fullerenes[23] leads to the hybridization of the dispersion, which increases with increasing periodicity and surface coverage of fullerenes as seen from comparing Figs. 7(a) – 7(c). Note, the hybridization effect on the dispersion seen for our nanobuds has been experimentally demonstrated for acoustic and nanophononic metamaterials and also have been predicted theoretically by solving the equations of motion for coupled oscillators.[12,13,53–57] It should also be noted that since the number of low frequency branches in the dispersion relation increases with increasing length of the computational domain, we have used similar lengths (∼4.5 nm) for the three computational represented in Figs. 7a–7c.

The flattening of the bands as observed from the dispersions lead to lowered group velocities and concomitantly to the large reduction in thermal conductivity. Note, for the entire frequency range, the hybridization effects are not readily observable in the density of states (see Fig. 7(d)) for the three different nanobuds represented in the dispersion. However, for the lower frequency range (0 – 3 THz), the MD-predicted DOS amongst the various computational domains do indeed show differences, which is consistent with the dispersion relations calculated via LD calculations.

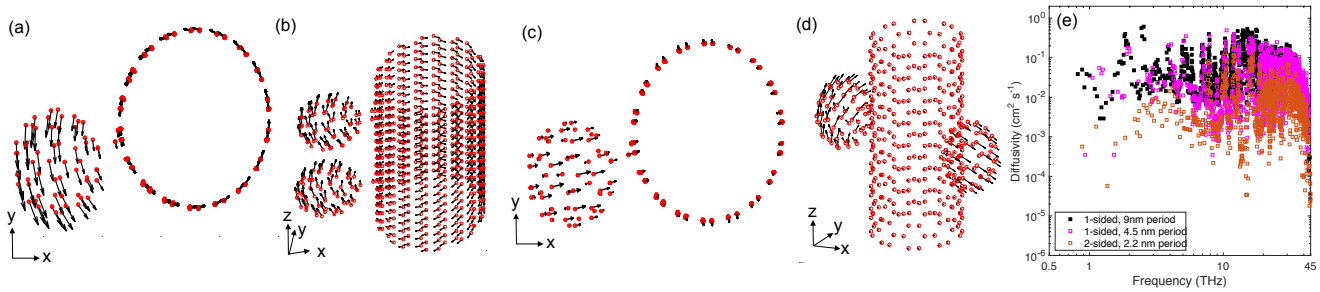

Figure 8. (a) Spatial components of the two dimensional eigenvectors at 0.179 THz for a 1-sided nanobud with 4.5 nm period length. (b) Visualization of three dimensional eigenvectors at 0.161 THz for 1-sided nanobud with 2.2 nm period length. (c) Two dimensional eigenvectors at 0.545 THz for a 1-sided nanobud with 4.5 nm period length and (d) three dimensional eigenvectors at 0.327 THz for a 2-sided nanobud with 4.5 nm period length showing resonant modes. (e) Comparison of mode diffusivities between 1-sided (9 nm period), 1-sided (4.5 nm period) and 2-sided (2.2 nm period) nanobuds.

To visualize the hybridization effects in our functionalized CNTs, we plot the vibrational eigenmodes for our various structures in Fig. 8. The arrows indicate the direction and magnitude of the particular eigenmode. Figure 8(a) shows the 2-dimensional plot of the eigenvectors in a 1-sided (4.5 nm period) nanobud for a 0.179 THz frequency. This is lower in frequency from the nearest hybridized mode as circled in Fig. 7(a). For this eigenmode, all atoms vibrate with the same amplitude and with a unified motion as shown by the arrows. Similarly, Fig. 8(b) shows the unified motion of atoms for a 1-sided nanobud with 2.2 nm period length at 0.161 THz frequency. The eigenvectors of the hybridized modes at 0.327 THz and 0.545 THz are shown in Fig. 8(c) and 8(d), respectively. The mismatch in the vibrational amplitudes in the fullerene resonators and the underlying CNT causes only the atoms in the fullerene molecules to vibrate at that frequency and the atoms in the main CNT do not participate in the eigenmode. This is clearly demonstrated by the negligible magnitudes of the eigenvectors (as shown in the 2-dimensional and 3-dimensional plots in Figs. 8(c) and 8(d)). These localized modes are characterized by the flat bands with reduced group velocities in the dispersion relations.

Next, to investigate the effect of hybridization on the entire spectrum, we calculate the diffusivities of the modes for the different structures according to the Allen-Feldman theory, which computes the contribution from diffusive and non-propagating modes as detailed in the earlier section.[39,40] Figure 8(e) shows the spectral diffusivities for 9 nm (1-sided), 4.5 nm (1-sided) and 2.2 nm (2-sided) nanobuds. There are two aspects of the data that are worth noting. First, as expected, the diffusivities of the modes gradually decrease with decreasing period length and increasing surface coverage of fullerenes on the CNT. Second, the diffusivities of the entire spectrum of modes are reduced with increased functionalization, reinstating our assertion that both the subwavelength and superwavelength frequencies are affected by the resonators.

The proposed functionalization of individual CNTs to reduce the thermal conductivity has several advantages. We have shown that the inclusion of fullerenes leads to the entire frequency spectrum showing the characteristic band flattening, and therefore the resonant structures can effectively lower the group velocities of nearly the entire vibrational bandwidth. Whereas, approaches to reduce thermal conductivity by engineering defect and impurity scattering usually only targets the high frequency vibrations and are thus not able to lower the contributions from low frequency phonons.[5,58–60] Furthermore, it has been shown that the height of the resonators can be modified to tune the resonant frequencies at the lower end of the spectrum;[13,14] the fullerenes attached to the CNT surface can be converted into tubular branches via treatment of electron beam irradiation,[23] thus providing an extra knob to tune the thermal conductivity of individual single-walled CNTs through manipulating the height of the resonators.

The main advantage of our approach to lower the thermal conductivity is the unique opportunity to simultaneously adjust the electronic and thermal properties of the nanobud structures. In this regard, a recent study based on density functional theory has suggested that the electronic properties of nanobuds are highly tunable by changing the surface coverage of fullerenes on the sidewall of CNTs.[33] This provides an exceptional avenue to optimize the thermoelectric efficiency by lowering the thermal conductivity while enhancing the electronic conductivity.

IV. CONCLUSIONS

In summary, we have performed atomistic simulations to reveal the unique thermal properties of CNTs funtionalized with fullerenes. To this end, we utilize the concept of resonant hybrid modes to demonstrate that the thermal conductivities of these organic compounds can be tuned in a wide range spanning an order of magnitude at 300 K. In contrast to the well known method of reducing thermal conductivity via scattering of high frequency vibrations, the resonant hybridization method targets low frequency phonons that contribute significantly to heat transport. This is achieved via hybridization between the modes of the fullerene and the underlying CNT, which forms resonant phonon band anticrossings due to the inclusion of the strongly bonded fullerene molecules. The strength of the hybridization effect can be increased with in-

creasing periodicity and surface coverage of fullerenes, thus offering a platform for user defined thermal transport in these novel material systems. This work provides a baseline for future research on the fundamental science of energy transport in organic-based low dimensional materials that utilize concepts of nanophononic materials and for the integration of 'nanobuds' in device applications.

ACKNOWLEDGEMENT

We would like to thank the Army Research Office for support (Grant No. W911NF-16-1-0320).

* ag4ar@virginia.edu
† phopkins@virginia.edu

[1] D. G. Cahill, W. K. Ford, K. E. Goodson, G. D. Mahan, A. Majumdar, H. J. Maris, R. Merlin, and S. R. Phillpot, Journal of Applied Physics **93**, 793 (2003).
[2] D. G. Cahill, P. V. Braun, G. Chen, D. R. Clarke, S. Fan, K. E. Goodson, P. Keblinski, W. P. King, G. D. Mahan, A. Majumdar, H. J. Maris, S. R. Phillpot, E. Pop, and L. Shi, Applied Physics Reviews **1**, 011305 (2014).
[3] Y. K. Koh and D. G. Cahill, Phys. Rev. B **76**, 075207 (2007).
[4] K. T. Regner, D. P. Sellan, Z. Su, C. H. Amon, A. J. H. McGaughey, and J. A. Malen, Nature Communications **4**, 1640 EP (2013).
[5] J. Garg, N. Bonini, B. Kozinsky, and N. Marzari, Phys. Rev. Lett. **106**, 045901 (2011).
[6] L. Chen, J. L. Braun, B. F. Donovan, P. E. Hopkins, and S. J. Poon, Applied Physics Letters **111**, 131902 (2017), https://doi.org/10.1063/1.4986884.
[7] C. Hua and A. J. Minnich, Semiconductor Science and Technology **29**, 124004 (2014).
[8] W. Kim, J. Zide, A. Gossard, D. Klenov, S. Stemmer, A. Shakouri, and A. Majumdar, Phys. Rev. Lett. **96**, 045901 (2006).
[9] R. Cheaito, C. A. Polanco, S. Addamane, J. Zhang, A. W. Ghosh, G. Balakrishnan, and P. E. Hopkins, Phys. Rev. B **97**, 085306 (2018).
[10] Y. K. Koh, Y. Cao, D. G. Cahill, and D. Jena, Advanced Functional Materials **19**, 610 (2009).
[11] Z. Liu, J. Mao, T.-H. Liu, G. Chen, and Z. Ren, MRS Bulletin **43**, 181 (2018).
[12] B. L. Davis and M. I. Hussein, Phys. Rev. Lett. **112**, 055505 (2014).
[13] H. Honarvar and M. I. Hussein, Phys. Rev. B **93**, 081412 (2016).
[14] S. Xiong, K. Sääskilahti, Y. A. Kosevich, H. Han, D. Donadio, and S. Volz, Phys. Rev. Lett. **117**, 025503 (2016).
[15] P. Wang, F. Casadei, S. Shan, J. C. Weaver, and K. Bertoldi, Phys. Rev. Lett. **113**, 014301 (2014).
[16] P. Kim, L. Shi, A. Majumdar, and P. L. McEuen, Phys. Rev. Lett. **87**, 215502 (2001).
[17] M. Fujii, X. Zhang, H. Xie, H. Ago, K. Takahashi, T. Ikuta, H. Abe, and T. Shimizu, Phys. Rev. Lett. **95**, 065502 (2005).
[18] C. Yu, L. Shi, Z. Yao, D. Li, and A. Majumdar, Nano Letters **5**, 1842 (2005).
[19] A. D. Avery, B. H. Zhou, J. Lee, E.-S. Lee, E. M. Miller, R. Ihly, D. Wesenberg, K. S. Mistry, S. L. Guillot, B. L. Zink, Y.-H. Kim, J. L. Blackburn, and A. J. Ferguson, Nature Energy **1**, 16033 EP (2016).
[20] M. A. Panzer, H. M. Duong, J. Okawa, J. Shiomi, B. L. Wardle, S. Maruyama, and K. E. Goodson, Nano Letters **10**, 2395 (2010).
[21] B. A. Cola, J. Xu, C. Cheng, X. Xu, T. S. Fisher, and H. Hu, Journal of Applied Physics **101**, 054313 (2007).
[22] A. Modi, N. Koratkar, E. Lass, B. Wei, and P. M. Ajayan, Nature **424**, 171 EP (2003).
[23] B. I. Kharisov, Recent Patents on Nanotechnology **11**, 235 (2017).
[24] A. G. Nasibulin, P. V. Pikhitsa, H. Jiang, D. P. Brown, A. V. Krasheninnikov, A. S. Anisimov, P. Queipo, A. Moisala, D. Gonzalez, G. Lientschnig, A. Hassanien, S. D. Shandakov, G. Lolli, D. E. Resasco, M. Choi, D. Tománek, and E. I. Kauppinen, Nature Nanotechnology **2**, 156 EP (2007).
[25] A. G. Nasibulin, A. S. Anisimov, P. V. Pikhitsa, H. Jiang, D. P. Brown, M. Choi, and E. I. Kauppinen, Chemical Physics Letters **446**, 109 (2007).
[26] X. Zhu and H. Su, Phys. Rev. B **79**, 165401 (2009).
[27] H. Su, W. A. G. III, and Y. Zhao, Nanotechnology **17**, 5691 (2006).
[28] C. Bhat, D. P. Brown, C. Chen, B. F. Mikladal, L. Ó. Súilleabháin, E. L. Soininen, D. Tian, I. Varjos, and X. Zhan, SID Symposium Digest of Technical Papers **46**, 1012 (2015), https://onlinelibrary.wiley.com/doi/pdf/10.1002/sdtp.10337.
[29] J. Tersoff, Phys. Rev. B **37**, 6991 (1988).
[30] J. Tersoff, Phys. Rev. B **39**, 5566 (1989).
[31] S. Plimpton, Journal of Computational Physics **117**, 1 (1995).
[32] J. D. Gale and A. L. Rohl, Molecular Simulation **29**, 291 (2003).
[33] X. Wu and X. C. Zeng, ACS Nano **2**, 1459 (2008).
[34] M. P. Allen and D. J. Tildesley, *Computer simulation of liquids (Oxford Science Publications)*, reprint ed., Oxford science publications (Oxford University Press, 1989).
[35] A. McGaughey and M. Kaviany, International Journal of Heat and Mass Transfer **47**, 1783 (2004).
[36] A. McGaughey and M. Kaviany, International Journal of Heat and Mass Transfer **47**, 1799 (2004).
[37] A. J. H. McGaughey, *Phonon Transport in Molecular Dynamics Simulations: Formulation and Thermal Conductivity Prediction*, Ph.D. thesis, University of Michigan (2004).
[38] J. M. Larkin and A. J. H. McGaughey, Phys. Rev. B **89**, 144303 (2014).
[39] P. B. Allen and J. L. Feldman, Phys. Rev. B **48**, 12581 (1993).
[40] J. M. Larkin and A. J. H. McGaughey, Journal of Applied Physics **114**, 023507 (2013).
[41] J. R. Lukes and H. Zhong, Journal of Heat Transfer **129**, 705 (2006).
[42] J. F. Moreland, Microscale Thermophysical Engineering **8**, 61 (2004), https://doi.org/10.1080/10893950490272939.
[43] S. Maruyama, Microscale Thermophysical Engineering **7**, 41 (2003), https://doi.org/10.1080/10893950390150467.
[44] R. N. Salaway and L. V. Zhigilei, International Journal of Heat and Mass Transfer **70**, 954 (2014).
[45] T. Kodama, M. Ohnishi, W. Park, T. Shiga, J. Park, T. Shimada, H. Shinohara, J. Shiomi, and K. E. Goodson, Nature Materials **16**, 892 EP (2017).
[46] D. W. Brenner, O. A. Shenderova, J. A. Harrison, S. J. Stuart, B. Ni, and S. B. Sinnott, Journal of Physics: Condensed Matter **14**, 783 (2002).
[47] D. W. Brenner, Phys. Rev. B **42**, 9458 (1990).

[48] J. X. Cao, X. H. Yan, Y. Xiao, and J. W. Ding, Phys. Rev. B **69**, 073407 (2004).
[49] J. M. Ziman, *Electrons and Phonons* (Clarendon Press, Oxford, 1960).
[50] S. J. Stuart, A. B. Tutein, and J. A. Harrison, The Journal of Chemical Physics **112**, 6472 (2000), https://doi.org/10.1063/1.481208.
[51] L. Xu, N. Wei, Y. Zheng, Z. Fan, H.-Q. Wang, and J.-C. Zheng, J. Mater. Chem. **22**, 1435 (2012).
[52] W. M. Ji, L. W. Zhang, and K. M. Liew, EPL (Europhysics Letters) **121**, 56001 (2018).
[53] N. Boechler, J. K. Eliason, A. Kumar, A. A. Maznev, K. A. Nelson, and N. Fang, Phys. Rev. Lett. **111**, 036103 (2013).
[54] P. J. Beltramo, D. Schneider, G. Fytas, and E. M. Furst, Phys. Rev. Lett. **113**, 205503 (2014).
[55] L. Novotny, American Journal of Physics **78**, 1199 (2010).
[56] T. Zhu, K. Swaminathan-Gopalan, K. J. Cruse, K. Stephani, and E. Ertekin, Advanced Functional Materials , 1706268 (2018), 1706268.
[57] E. A. Garova, A. A. Maradudin, and A. P. Mayer, Phys. Rev. B **59**, 13291 (1999).
[58] M. Roufosse and P. G. Klemens, Phys. Rev. B **7**, 5379 (1973).
[59] P. Klemens (Academic Press, 1958) pp. 1 – 98.
[60] A. Giri, J. L. Braun, C. M. Rost, and P. E. Hopkins, Scripta Materialia **138**, 134 (2017).